Carbon nanotube coatings as used in strain sensors for composite tanks

Steve Trigwell[1]*, Sarah Snyder[1], Walt Hatfield[2], Enkeleda Dervishi[3], Alexandru S. Biris[3]

[1]Sierra Lobo, Inc., [2]Stinger Ghaffarian Technologies, Inc.,
Kennedy Space Center, FL 32899

[3]Nanotechnology Center, University of Arkansas at Little Rock, 2801 S. University Ave., Little Rock, AR 72204

*Address for correspondence: steven.trigwell-1@nasa.gov
321-867-1222

Abstract

The next generation of cryogenic fuel tanks, crew habitats and other components for future spacecraft will focus on the use of lightweight carbon fiber composite materials. A critical issue in the design and optimization of such tanks and structures will be in structural health monitoring, however, current strain sensors have limitations. In this study, a novel carbon nanotube thin film was applied to carbon fiber composites for structural monitoring. Applying a load using a 3-point bend test to simulate bowing of a tank wall, induced significant increases in the film's electrical resistance at small deflections. Upon release of the load, the resistance returned to its approximate start value and was reproducible over multiple tests. The results show that a carbon nanotube thin film has great potential for the health monitoring of composite structures.

Introduction

After the retirement of the space shuttle fleet, the next generation of reusable launch vehicles (RLV) will require new and innovative materials for weight and cost savings. One of the major components of an RLV are the cryogenic tanks for propellant storage. The development of new lightweight tanks has been researched for several years, with lightweight carbon fiber composites

being the major focus [1, 2]. However, during development of composite cryogenic tanks, there have been a couple of incidents involving dramatic tank failure during testing [3,4, 4a]. Notice of impending failure would have prevented the cost in injuries and damage to facilities. Current structural monitoring technologies typically use metal foil strain gauges but which have significant limitations such as measuring strain in designated directions and locations, and susceptible to drifting due to temperature sensitivity. Also traditional strain gages have an extremely high failure rate therefore are not well suited for long term use to determine the "health" of a composite structure. Furthermore, many structures such as airframes and cryogenic tanks do not allow access to place or change strain gages if failed. Ever since their discovery, CNTs have been researched extensively due to their exceptional electrical and mechanical properties as potential candidates for many applications such as nano-sensors, nanoelectromechanical devices, switches, carbon nanotube-based oscillators and many more [5-9].

The use of carbon nanotube (CNT) films for strain sensors for structural health monitoring have been proposed and tested [10-14] with excellent results, however in these cases, no specific applications were addressed. Development of an embedded strain sensor in a composite structure for use in future transportation vehicles will allow static and dynamic responses without compromising the host structure was reported by Park et al. [12]. One concern has been that CNT films are sensitive to temperature that may introduce errors in a widely varying temperature environment. Results from Vemura et al. [14] showed multi-wall CNT (MWCNT) films exhibited a decrease in resistivity with increasing temperature, but it was stable and predictable, varying by only 0.0217 ohm for a temperature change of 21.1 °C to 35 °C. Similarly, Koratkar et

al. [15] observed a small decrease in resistance with increasing temperature of a vertically aligned MWCNT film investigated in the temperature range -150 °C to 300 °C.

Additionally, carbon nanotubes and especially multi-wall carbon nanotubes (MWCNTs) were incorporated into different type of polymers creating new nano-composite materials with enhanced mechanical and electrical properties [16,17]. It is important to mention that the parameters such as nanotube crystallinity, length, concentration, interaction between the nanotubes and the polymer matrix strongly affect the mechanical properties of these new carbon nanotube-reinforced polymer composites [18,19]. Carbon nanotubes synthesized by chemical vapor deposition were found to be very tough and strong and have an extremely high Young's moduli (in the TPa range) by several groups around the world [20, 21]. Wong et al used an atomic force microscope to determine the mechanical properties of isolated MWCNTs [22]. Through a series of continued bending movements, the Young's modulus of the carbon nanotubes was measured to be about 1.28 TPa independent of the nanotube diameter [22].

To characterize a series of individual MWCNTs, Yu et al performed a tensile-loading experiment within a scanning electron microscope, where the highest tensile strength and the Young's modulus of the outer most tube of a MWCNT were found to be 63 GPa and 950 GPa respectively [23]. Furthermore, the static and dynamic mechanical deflections of MWCNTs performed in a transmission electron microscope, established that the elastic bending modulus was found to decrease from 1 to 0.1 TPa as the diameter of the nanotubes increased from 8 to 40 nm [24].

Based on CNT's remarkable properties, they have potential of serving as active materials in a number of applications that require the continuous monitoring of the integrity of large-scale structures such as composite tanks. Their superelastic properties also mean they can be bent to

large degrees and recover. Using the piezoresistivity of CNTs, i.e. change in resistance with strain, and the possibility of integrating the CNTs in large area films, indicated the possibility of using them as a novel strain sensor for high pressure tanks and devices. In the case of a composite tank, there is a need to sense small changes in surface strain that may not be detected by existing strain gauges. Current strain gauges are limited by only being able to measure the strains on structural surfaces in designated directions and locations and do not have the sensitivity to detect small strains.

Here we show that carbon nanotube films have the ability to very accurately detect minor surface deformations of the supporting substrates by a simple change in their electrical resistivity and current-voltage (I-V) diagrams. This approach can be used for a large number of applications that range from high pressure tanks to avionics and space explorations. The elegance of the method consists in the simple carbon nanotube film deposition by air-spraying, and the connection of the film to a continuous voltage difference. The current can be continuously monitored and any change is immediately related to a stretching of the films and concurrently a possible deformation of the substrate. In this study, the coupons were subjected to a 3-point bend test to simulate the bowing of the side of a tank. In pressure testing large tanks, bowing, or strain in weak points may not be obvious, and there is the need to detect very small changes in the structural integrity.

Experimental Design

Catalyst Preparation

The Fe-Co/$CaCO_3$ (2.5:2.5:95 wt.%) catalyst system which was utilized for the MWCNT growth was prepared as previously described [25]. The $Fe(NO_3)_3 \cdot 9H_2O$ and $Co(CH_3COO)_2 \cdot 4H_2O$ metal salts were completely dissolved in DI water under continuous stirring. Next, the $CaCO_3$

support was added to this mixture and the solution was stirred and subsequently sonicated for 30 minutes. In order to avoid the release of CO_2, ammonia was added to the final solution until its pH reached 7.5. A steam bath set up was used to evaporate the water while the solution was constantly stirred. Lastly, the catalyst system was dried overnight at 100 °C and calcinated at 600 °C for 2 hours.

Carbon nanotube Synthesis

MWCNTs were synthesized on the Fe-Co/$CaCO_3$ catalyst system using a Radio Frequency (RF) chemical vapor deposition (CVD) method [25]. The catalyst system (100 mg) was deposited into a thin layer on a graphite susceptor which was positioned inside of a quartz tube. The latter was placed at the center of the RF generator and purged with nitrogen at 200 ml/min for 10 minutes. Next, the RF generator was turned on and when the temperature reached 720 °C, acetylene was introduced at 3.3 ml/min for 30 minutes. Finally, the product was allowed to cool down under nitrogen for 10 minutes.

The as-produced MWCNTs were purified using diluted nitric acid (HNO_3)/H_2O (1:1 by volume) solution. The acid nanotube mixture was continuously stirred overnight at 100 °C and during this purification process carboxylic functional groups (COOH) are attached on the surface of the carbon nanotubes. Next, the mixture was filtered through an Isopore membrane filter with 0.2 μm pore size (from Millipore) and was washed with DI water until the pH was neutral and all the acid was completely removed.

Carbon Nanotube Characterization

The purified MWCNTs were characterized by transmission electron microscopy (TEM), thermo-gravimetric analysis (TGA), and Raman scattering spectroscopy. The deposited film was

characterized by secondary electron spectroscopy (SEM) and x-ray photoelectron spectroscopy (XPS).

Low and high resolution TEM images of carbon nanotubes were obtained using on a field emission JEM-2100F TEM (JEOL Inc.) supplied with a CCD camera. The acceleration voltage was set to 100 kV. The functionalized MWCNTs were homogeneously dispersed in iso-propanol and tip sonicated for 30 minutes. Next, a few drops of the suspension were deposited on the TEM grid and air dried before analysis.

A Mettler Toledo TGA/SDTA 851e was utilized to perform thermo-gravimetric analyses and determine the thermal properties of MWCNTs. Approximately 3 mg of the purified MWCNTs was heated from 25 to 800 ^{o}C at a heating rate of 5 ^{o}C /min, under air flow of 150 ml/min.

Raman scattering studies of the MWCNTs were performed at room temperature using Horiba Jobin Yvon LabRam HR800. Before each analysis, the Raman spectrometer was calibrated using a silicon wafer with a known Raman peak at 521 cm^{-1}. The He-Ne laser (633 nm) with a power of 5 mW was utilized as an excitation source.

A JEM-7500F field emission SEM was used to take low and high resolution images of the as-deposited CNT films. A low accelerating voltage of 2 kV was used to prevent charging up of the CNTs in the films at a working distance of 7 - 11 mm.

XPS analysis was performed on a Thermo Scientific K-Alpha spectrometer utilizing an Al kα x-ray source with energy of 1486.6 eV at a background pressure of 1 x 10^{-9} mbar. The spot size used was 400 µm. Survey scans were acquired to obtain the relative elemental composition of the as-received carbon composite coupon surface, and of the CNT film after deposition onto the coupons. The relative elemental atomic concentrations were calculated using sensitivity factors provided by the manufacturer with the instrument. Narrow scans at higher energy resolution of

the C1s peak were performed on the as-received coupon and after CNT film deposition to determine chemical state information of the film. The C1s peak was reference to the C-C/C-H peak at 284 6 eV.

Carbon Nanotube Deposition

Since carbon nanotubes are inherently hydrophobic and tend to agglomerate due to the strong Wan der Waal forces, usually they have to be functionalized with different functional groups or mixed with various surfactants in order to achieve a homogenous dispersion. MWCNTs were functionalized through a nitric acid treatment to improve their water solubility and ensure a more uniform solution. The purified MWCNTs were added to 30 ml of DI H_2O at 0.3 mg/ml concentration and tip sonicated for one hour. The homogenous aqueous suspension was deposited on coupons fabricated from carbon composite material from a cryogenic tank of dimensions 100 mm x 50 mm x 3.33 mm through an airbrushing technique as previously described [26]. An optical micrograph of the coupon surface is shown in Figure 1where the woven construction of the carbon fibers is evident. Approximately, 90 ml of the nanotube suspension was deposited on each coupon. During the deposition process, the coupons were placed on a heating stage and heated up at 100 ^{o}C allowing the water to evaporate, while leaving behind nanotubes uniformly deposited on the coupon surface. Figure 2 shows SEM images of the deposited CNT film at low and high magnifications.

Strain testing experimental set up

The coupons were masked with a 37.5 mm strip across the center of the film coated side, and then a thin copper film was applied by sputter deposition to provide conductive connection points for the wires. Wires were silver solder connected to points on the copper film on each side of the CNT film so they were within the anvil span of the 3-point flexure fixture on the Instron,

and encapsulated with an epoxy to provide extra strength, as shown in Figure 1. Areas at the end of each coupon were then scraped with a scalpel blade to remove the unnecessary copper film (Fig. 3) so that the composite coupon could be mounted to the 3-point bend test fixture without shorting the connections and CNT film to ground, as shown in Figure 4. The 3-point bend tests were performed on Instron Model 3344 2kN table top tensile tester equipped with a flexure fixture utilizing Series IX/s software. The tests were performed at a speed of 0.05 mm/s to a maximum load of 2 kN. Preliminary testing on blank coupons to the maximum load of 2 kN showed an extension (deflection of the coupon) of 2.61 mm with a flexure stress of 355.45 MPa and flexure strain of 1.26 %. A low voltage of 100 mV was applied across the film, and the current through the CNT film was monitored using a precision electrometer (Keithley Model 6514).

Results and Discussions

Crystallinity, purity, wall number and tube length are some of the main parameters that greatly influence the optical, thermal, mechanical and electrical properties of carbon nanotubes. In particular carbon nanotubes with high crystallinity and very few structural defects are shown to possess higher electrical, thermal, optical and mechanical properties [27, 28]. Long carbon nanotubes are shown to exhibit better electrical properties when compared to the shorter ones. Wall number also plays a very important role on the opto-electronic, thermal and electrical properties of carbon nanotubes leading to the need to synthesize species of nanotubes with specific number of walls (1, 2, 3, multi) for applications that require the use of these materials for electrically conductive films [29-32]. The mechanical properties are also dependent on the type of CNTs, where MWCNTs were found to have higher Young's modulus than SWCNTs due to difference in the wall number, tube diameter and the van der Waals forces present between the

tubes [33, 34]. Furthermore, impurities such as metal nano-particles that are present between the carbon nanotube bundles hinder their performance in several applications. Usually, nanotubes with higher purities demonstrate much better properties when compared to the ones containing various number of impurities such as catalytic metal nano-particles and amorphous carbon [35]. Raman spectroscopy has also demonstrated that the presence of impurities was found to influence the structural properties of CNTs [36]. Therefore, when utilizing carbon nano-materials for various applications, it is important to thoroughly characterize their properties by techniques such as microscopy, spectroscopy and thermal gravimetrical analysis.

TEM analysis indicated that the MWCNTs utilized in this manuscript have outer diameters varying between 15-30 nm and an average length of over 6 microns. The low and high resolution TEM images of MWCNTs are shown in Figures 5 (a) and (b) respectively. The high resolution TEM image indicates the presence of a MWCNT (shown by the arrow) with an inner diameter of 5 nm and an outer diameter of 19 nm.

Thermo-gravimetrical analyses (TGA) were performed to determine the purity of MWCNTs. Figure 6 (a) shows the weight loss profile of the functionalized MWCNTs, revealing that their purity was found to be slightly higher than 98 %. The remaining quantity (less than 2%) corresponds to the catalyst nano-particles that are still present within the bundles of carbon nanotubes or entrapped in the inner most cylinder of the MWCNTs and could not be removed after the first purification process. The TGA curve as well as its first derivative (shown in the inset of Figure 4 (a)) indicate that the decomposition temperature of the purified nanotubes was found to be at around 587 ^{o}C. It has been reported that the combustion temperature of the CNTs depends on their morphological properties, where usually nanotubes with higher crystallinity decompose at a higher temperatures [37].

Raman Spectroscopy is a non-destructive and widely used technique to characterize various carbon nano-structures. The D, G and 2D band are three characteristic bands found in the high frequency domain of the MWCNT Raman scattering spectrum. The D band is positioned between 1300 and 1380 cm^{-1} and is correlated with the presence of defects, impurities, amorphous carbon or other carbonaceous products, which are present in the carbon nanotube sample [38]. The G band, or also known as the tangential band, is present between 1500 and 1630 cm^{-1} and it corresponds to the E_{2g} stretching modes in the graphite plane [39]. The last band present in the high frequency domain of the carbon nanotube spectra is the 2D band or the second-order harmonic of the D band. The latter is present between 2450 and 2650 cm^{-1} and it is often associated with the degree of the nanotube crystallinity [40]. Figure 4 (b) shows the Raman scattering spectrum of the purified MWCNTs collected with 633 nm He-Ne laser. The inset shows a high resolution TEM image of a MWCNT with an outer diameter of 22 nm. The relative high intensity of the 2D band indicates the presence of MWCNTs with high crystallinity. These findings were found to be in a very in good agreement with the TGA results.

The SEM images of the CNT deposited film (Fig. 2) showed an even distribution of the CNTs within the film. Fig. 2(b) showed the CNTs have a good uniform size consistent with the TEM analysis and also a good weave between CNTs providing a good conductive path through the coating. No impurities or defects were observed in the SEM images.

The XPS spectra are shown in Figure 7. Fig. 7(a) shows the C1s peak of the as-received composite coupon. The relative elemental composition of the uncoated surface is presented in Table 1. The data shows the presence of alcohol or ester (C-O) and aldehyde or ketone (C=O) groups [41] plus fluoropolymer, along with minor traces of contaminants. For the CNT coating, predominantly carbon, plus minor oxygen was detected (Table 1), which is expected of a surface

exposed to the environment. The C1s peak (Fig. 7(b), shows a typical C1s peak of that of graphite at ~ 284.4 eV [42] with the characteristic tail towards higher binding energy. No contaminants and lack of carbon functional groups indicates the high purity of the CNT coating. Prior to the 3-point bend test, the CNT film resistance was measured under no load conditions to evaluate the stability of the films as a function of humidity. A fixed voltage of 100 mV was applied to the films and the current through the film was monitored as a function of relative humidity (RH%) utilizing the environmental chamber in the laboratory. The change in the measured current is in direct proportion to the change in resistivity. The results are shown in Figure 8 where a linear correlation between the increase in the RH% and decrease in current was observed. Secondly, the measured current as a function of fixed RH% was measured and showed good stability (Fig. 9) over a period of 2 hours. The values for 2% RH were less stable but was probably due to the inaccuracy in measuring that low a RH. However, across the RH range monitored, the current changed by less than 1 mA, indicating that as long as the RH% was known and stable, reproducible and reliable data can be obtained.

The coupon was then subjected to the 3-point bend test at a constant RH % to the maximum deflection measurement of 2.61 mm, as shown in Figure 4b. Again a fixed voltage of 100 mV was applied to the coupon and the current through the CNT film was monitored on an electrometer as a function of the applied stress to a maximum deflection of the coupon. The film resistance as a function of the applied stress was therefore calculated. Four total runs were performed on one coupon. A linear correlation between the applied stress and increase in the CNT film resistance was determined (Fig. 10). The resistance values rose from 6 to 7 ohm at the start to 16-22 ohm at the maximum deflection. The small deviations between runs may be due to humidity fluctuations in the laboratory that could not be controlled as well as in the

environmental chamber. At 52 seconds at maximum load, the load was removed and the resistance value of the film returned to within a few % of the original values, as shown in Table 2. This recovery showed that the superelastic component of the CNT film had not been exceeded, the deflection of 2.61 mm of the coupon being due to the load limit of the instrument. The change in the current for a fixed voltage of 100 mV as a function of humidity, as shown in Figures 8 and 9, corresponded to a maximum change in starting resistance of +/- 0.5 ohm. This is small compared to the total change in resistance at maximum deflection indicating that resistance changes of greater than 1 ohm were significant showing that deflections as low as 0.5 mm could be detected.

Future research will focus on a coating for the films to protect them from the environment, and incorporating them into the composite itself. Furthermore, development of CNTs themselves that mimic the strength of the weakest carbon fiber (or slightly less) for incorporation in the composite structure itself could be used so that when the ultimate strength of the CNT was exceeded and the CNT broke, the resistance would be greatly and permanently changed indicating potential carbon fiber breakage and impending failure of the tank of structure. With future research underway to improve and develop ultralight linerless composite tanks for aircraft, launch vehicles, and in space propulsion [43, 44], the need for health monitoring for these tanks becomes critical.

Conclusions

Data from the experiments showed that small deflections of a carbon composite coupon simulating the bowing of a tank wall could be easily detected using a MWCNT film. Due to the superelasticity of the MWCNT film, the resistance of the film returned to within a few percent the starting value and showed reproducible results over several runs. The films are also made up

of MWCNTs in random directions, so that the resistance could be monitored independent of direction. Such films could also be incorporated into the carbon fiber structure. The results indicate the feasibility of using CNT films as structural health monitoring of composite tanks and structures.

Acknowledgements

The authors wish to thank Judith McFall of ASRC Aerospace for help in the strain testing, and to Paul Hintze of NASA Kennedy Space Center for his assistance in the SEM photographs.

References

[1] T. DeLay, "Hybrid composite cryogenic tank structure", *NASA Tech Briefs*, Jan. 2011

[2] K. Ryan, J. Cronin, S. Arzberger, K. Mallick, and N. Munshi, "Prediction of pressure cycle induced microcrack damage in linerless composite tanks", *Proc. AIAA/ASME/ASCE/AMS/ASC Structures, Structural Dynamics, and Materials Conf.,* Newport RI, 2006. AIAA2006-2201.

[3] Final report of the X-33 liquid hydrogen tank test investigation team, Marshall Space Flight Center, Huntsville, AL, May 2000.

[4] Investigation of the cryogenic composite tank rupture type D/Close call mishap report, NASA IRIS Incident No. S-2008-359-00002, February 20, 2009.
http://kscsafety.ksc.nasa.gov/KSCSafetyMishaps.htm

[5] C. Li and T. W. Chou, "Atomistic Modeling of Carbon Nanotube-based Mechanical Sensors", *J. Intelligent Material Systems and Structures,* 17(3), pp. 247-254, 2006.

[6] H. G. Craighead, "Nanoelectromechanical Systems", *Science*, 290, 5496, pp. 1532-1535, 2000.

[7] A. Kis and A. Zettl, "Nanomechanics of carbon nanotubes" *Phil. Trans. R. Soc. A 13,* 366, 1870, pp. 1591-1611, 2008.

[8] E. Dervishi, Z. Li, Y. Xu, V. Saini, A. R. Biris, D. Lupu, and A. S. Biris, "Carbon Nanotubes: Synthesis, Properties, and Applications", *Particulate Science and Technology*, 27, pp.107–125, 2009.

[9] Y. Zhu and H. D. Espinosa, "An electromechanical material testing system for *in situ* electron microscopy and applications", *PNAS, 2005,* 102, 41, pp.14503–14508, 2005

[10] K.J. Loh, J.P. Lynch, and N.A. Kotov, "Conformable single-walled carbon nanotube thin film strain sensors for structural monitoring", *Proc. 5th International workshop on structural health monitoring*, Stanford, CA, Sept. 2005.

[11] I. Kang, M.J. Schulz, J.H. Kim, V. Shanov, and D. Shi, "A carbon nanotube strain sensor for structural health monitoring", *Smart Materials and Structures*, 15, pp. 737-748, 2006.

[12] M. Park, H. Kim, and J. Youngblood, "Strain-dependant electrical resistance of multi-walled carbon nanotube/polymer composite films", *Nanotechnology*, 19, 055705 (7pp) 2008.

[13] X. Li, C. Levy, and L. Elaadil, "Multiwalled carbon nanotube film for for strain sensing", *Nanotechnology*, 19, 045501 (7pp) 2008.

[14] S.M. Vemura, R. Wahi, S. Nagarajaiah, and P.M. Ajayan, "Strain sensing using a multiwalled carbon nanotube film", *J. Strain Analysis*, 44, pp. 555-562, 2009.

[15] N. Koratkar, A. Modi, E. Lass, and P. Ajayan, "Temperature effects on resistance of aligned multiwalled carbon nanotube films", *J. Nanosci. Nanotechnol.*, 4(7), pp. 744-748, 2004.

[16] W. Wang, P. Ciselli, E. Kuznetsov, T. Peijs, and A. H. Barber, "Effective reinforcement in carbon nanotube–polymer composites", *Phil. Trans. R. Soc. A* 13, 366, 1870, pp. 1613-1626, 2008.

[17] L. Tong, X. Sun, and P. Tan, "Effect of Long Multi-walled Carbon Nanotubes on Delamination Toughness of Laminated Composites", *J. Composite Materials,* 42(1), pp.5-23, 2008.

[18] A. B. Sulong, J. Park, N. Lee, and J. Goak, "Wear Behavior of Functionalized Multi-walled Carbon Nanotube Reinforced Epoxy Matrix Composites", *J. Composite Materials*, 40(21), pp. 1947-1960, 2006.

[19] Y. C. Zhang and X. Wang, "Hygrothermal Effects on Interfacial Stress Transfer Characteristics of Carbon Nanotubes-reinforced Composites System", *J. Reinforced Plastics and Composites,* 25(1), pp. 71-88, 2006.

[20] R. L. Jacobsen, T. M. Tritt, J. R. Guth, A. C. Ehrlich, and D. J. Gillespie, "Mechanical properties of vapor-grown carbon fiber", *Carbon,* 33(9), pp. 1217-1221, 1995.

[21] M. M. J. Treacy, T. W. Ebbesen, and J. M. Gibson "Exceptionally high Young's modulus observed for individual carbon nanotubes", *Nature* 381, pp. 678-680, 1996.

[22] E. W. Wong, P. E. Sheehan, and C. M. Lieber, "Nanobeam Mechanics: Elasticity, Strength, and Toughness of Nanorods and Nanotubes", *Science,* 277(5334), pp. 1971-1975, 1997.

[23] M-F. Yu, O. Lourie, M.J. Dyer, K. Moloni, T.F. Kelly, and R.S. Ruoff, "Strength and Breaking Mechanism of Multiwalled Carbon Nanotubes Under Tensile Load", *Science*, 287(5453), pp. 637-640, 2000.

[24] Philippe Poncharal, Z. L. Wang, Daniel Ugarte and Walt A. de Heer, "Electrostatic Deflections and Electromechanical Resonances of Carbon Nanotubes" *Science*, 283(5407), pp. 1513-1516, 1999.

[25] E. Dervishi, Z. Li , A. R. Biris, D. Lupu, S. Trigwell and A. S. Biris, "Morphology of Multi-Walled Carbon Nanotubes Affected by the Thermal Stability of the Catalyst System", *Chem. Mater.* 19, pp. 179-184, 2007.

[26] Z. Li, H. R. Kandel, E. Dervishi, V. Saini, Y. Xu, A. R. Biris, D. Lupu, G. J. Salamo, and A. S. Biris, "Comparative study on different carbon nanotube materials in terms of transparent conductive coatings", *Langmuir*, 24(6), pp. 2655-2662, 2008.

[27] R. Jin, Z. X. Zhou, D. Mandrus, I.N. Ivanov, G. Eres, J.Y. Howe, A.A. Puretzky, and D.B. Geohegan, "The effect of annealing on the electrical and thermal transport properties of macroscopic bundles of long multi-wall carbon nanotubes" *Physica ,B* 388, pp. 326-330, 2007

[28] S. I. Jung, S. H. Jo, H. S. Moon, J. M. Kim, D. S. Zang, and C. J. Lee, " Improved Crystallinity of Double-Walled Carbon Nanotubes after a high-temperature thermal annealing and their enhanced field emission properties", *J. Phys. Chem. C*, 111, pp. 4175-4179, 2007.

[29] E. Dervishi, Z. Li, V. Saini, R. Sharma, Y. Xu, M. K. Mazumder, A. S. Biris, S. Trigwell, A. R. Biris, D. Saini, and D. Lupu, "Multifunctional coatings with carbon nanotubes for electrostatic charge mitigation and with controllable surface properties", *IEEE Trans. Ind. Apps.*, 45(5), pp. 1547-1552, 2009.

[30] E. Dervishi, Z. Li, F. Watanabe, Y. Xu, V. Saini, A. R. Biris and A. S. Biris, "Thermally controlled synthesis of single-wall carbon nanotubes with selective diameters", *J. Mater. Chem.*, 19, pp. 3004–3012, 2009

[31] A.R. Biris, D. Lupu, A. Grüneis, P. Ayala, M.H. Rümmel, T. Pichler, Z. Li, I. Misan, E. Dervishi, Y. Xu, and A.S. Biris, "High quality double wall carbon nanotubes grown by a cold-walled radio frequency chemical vapor deposition process", *Chemistry of Materials*, 20(10), pp. 3466-3472, 2008

[32] Z. Li, H. R. Kandel, E. Dervishi, V. Saini, A. S. Biris, A. R. Biris and D. Lupu, "Does the wall number of carbon nanotubes matter as conductive transparent material?" *App. Physics Letts.*, 91, 053115, 2007 (3 pages).

[33] M. Meyyappan, 2005. *Carbon Nanotubes: Science and Applications.* Boca Raton, Fla.: CRC,

[34] E. Dervishi, Z. Li, Y. Xu, V. Saini, A. R. Biris, D. Lupu, and A. S. Biris, "Carbon Nanotubes: Synthesis, Properties, and Applications", *Particulate Science and Technology*, 27, pp.107–125, 2009.

[35] Z. Li, A. S. Biris, E. Dervishi, V. Saini, Y. Xu, A. R. Biris and D. Lupu, "Influence of impurities on the x-ray photoelectron spectroscopy and Raman spectra of single-wall carbon nanotubes", *J. Chem. Phys.*, 127, 154713 , 2007 (7 pages).

[36] L.E. McNeil, H. Park, J.P. Lu and M.J. Peters, "Effect of residual catalyst on the vibrational modes of single-walled carbon nanotubes," *J. Appl. Phys.* 96, pp. 5158-5162. 2004.

[37] G. S. B. McKee and K. S. Vecchio, "Thermogravimetric analysis of synthesis variation effects on CVD generated multiwalled carbon nanotubes", *J. Phys. Chem. B*, 110(3), pp.1179–1186, 2006.

[38] M. S. Dresselhaus and P. C. Eklund, "Phonons in carbon nanotubes", *Advances in Physics*, 49(6), pp. 705-814, 2000.

[39] E.F. Antunes, A.O. Lobo, E.J. Corat, V.J. Trava-Airoldi, A.A. Martin, and C. Veri´ssimo, "Comparative study of first- and second order Raman spectra of MWCNT at visible and infrared laser excitation", *Carbon,* 44, pp. 2202, 2006.

[40] M.S. Dresselhaus, G. Dresselhaus, R. Saito, and A. Jorio, "Raman spectroscopy of carbon nanotubes" *Physics Reports*, 409, pp. 47-99, 2005.

[41] D. Briggs, in "Practical Surface Analysis Volume 1 - Auger and X-ray Photoelectron Spectroscopy", D. Briggs and M.P. Seah (Eds.), John Wiley, Chichester, UK, 1990, p. 444.

[42] H. Ago, T. Kugler, F. Cacialli, W.R. Salaneck, M.S.P. Shaffer, A.H. Windle, and R.H. Friend, "Work functions and surface functional groups of multiwall carbon nanotubes", *J. Phys. Chem. B*, 103, pp. 8116-8121, 1999.

[43] K. Mallick, J. Cronin, K. Ryan, S. Arzberger, and N. Munshi, "An integrated systematic approach to linerless composite tank development", *Proc. 46th AIAA/ASME/ASCE/AMS/ASC Structure, Structural Dynamics and Materials Conference,* Austin, TX, 2005. AIAA 2005-2009.

[44] K. Ryan, J. Cronin, S. Arzbereger, K. Mallick, and N. Munshi, "Prediction of pressure cycle induced microcrack damage in linerless composite tanks", *Proc. 46th*

Figure captions

Figure 1: Optical photograph of the uncoated carbon fiber coupon surface showing the topography of the construction.

Figure 2: (a) Low resolution SEM image of the MWCNT coating on the coupon. (b) High resolution SEM image.

Figure 3: CNT coated composite coupon showing set-up for testing. The CNT film was scraped off each end of the coupon so there would be no electrical contact of the CNT film with the Instron anvil.

Figure 4: The CNT coated coupon as mounted in the Instron for the 3-point bend test at t=0 secs (a). The CNT coated coupon at the conclusion of the 3-point bend test at t=52 secs (b). Maximum deflection of the coupon was 2.61 mm.

Figure 5: (a) Low resolution TEM image of MWCNTs synthesized with acetylene. (b) High resolution TEM image.

Figure 6: (a) The weight loss profile of the MWCNTs obtained during thermo-gravimetric analysis and (inset) the first derivative of the TGA curve indicating the combustion temperature for the purified nanotubes. (b) Raman scattering spectra of the MWCNTs synthesized on the Fe-Co/$CaCO_3$ catalyst system, (inset) TEM image of a purified MWCNT.

Figure 7: (a) High resolution XPS spectrum of the C1s peak of the uncoated carbon fiber coupon surface showing the carbon species detected. (b) High resolution spectrum of the C1s peak of the MWCNT coating.

Figure 8: Current as measured through the CNT film at constant voltage as a function of relative humidity (RH%).

Figure 9: Current as measured through the CNT film at various RH% as a function of time.

Figure 10: Resistance change of the CNT film as a function of applied strain.

Table captions

Table 1: Relative atomic concentrations determined by XPS of the surface of the uncoated and MWCNT coated carbon fiber coupon.

Table 2: Resistance measurements across the film at the start, at maximum deflection, and after the load was removed for all four runs.

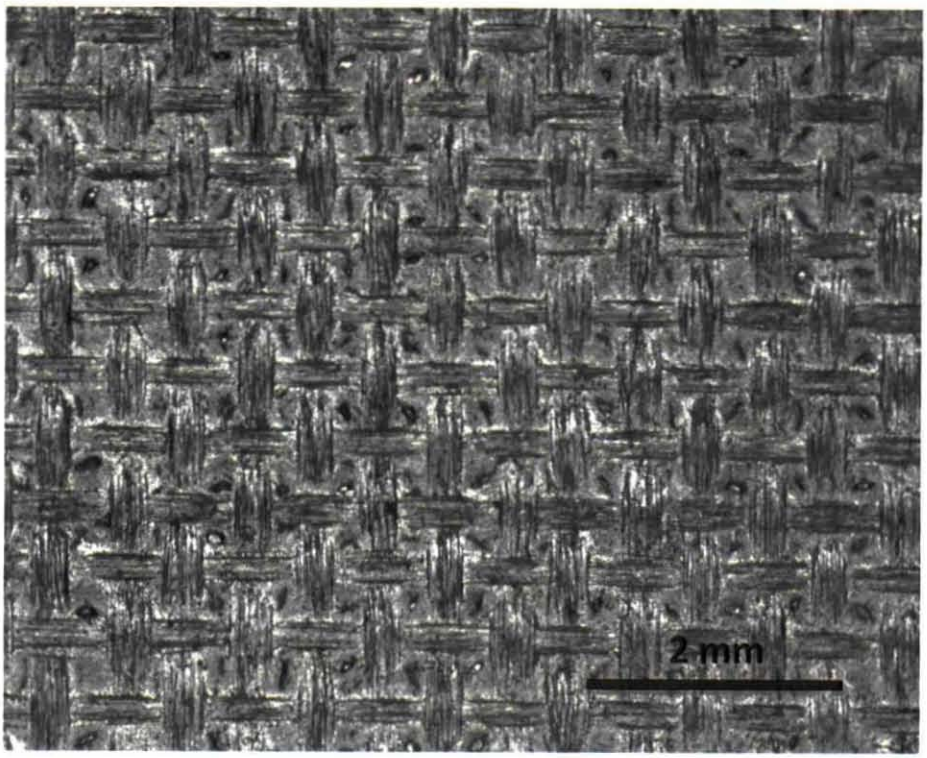
2 mm

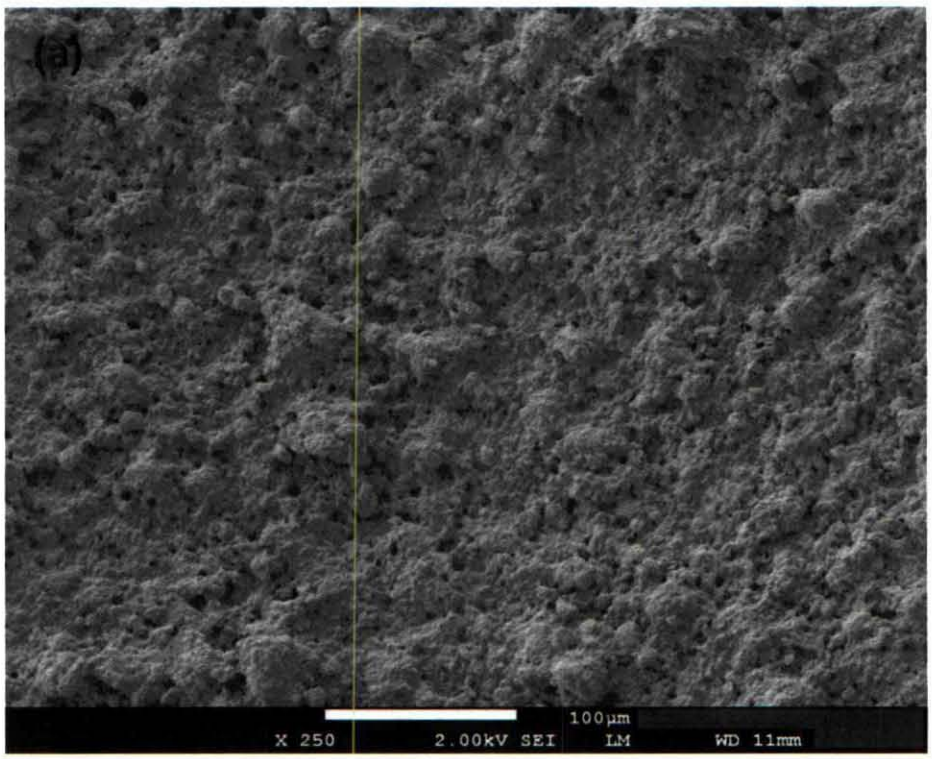
(a)
100µm
X 250 2.00kV SEI LM WD 11mm

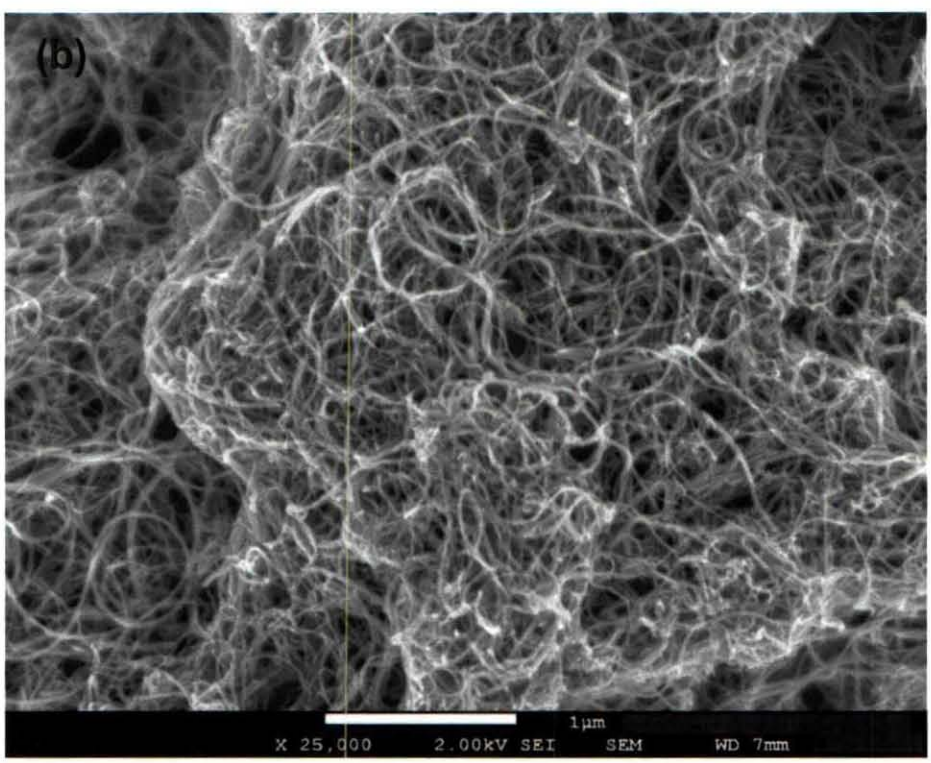
(b)
1µm
X 25,000 2.00kV SEI SEM WD 7mm

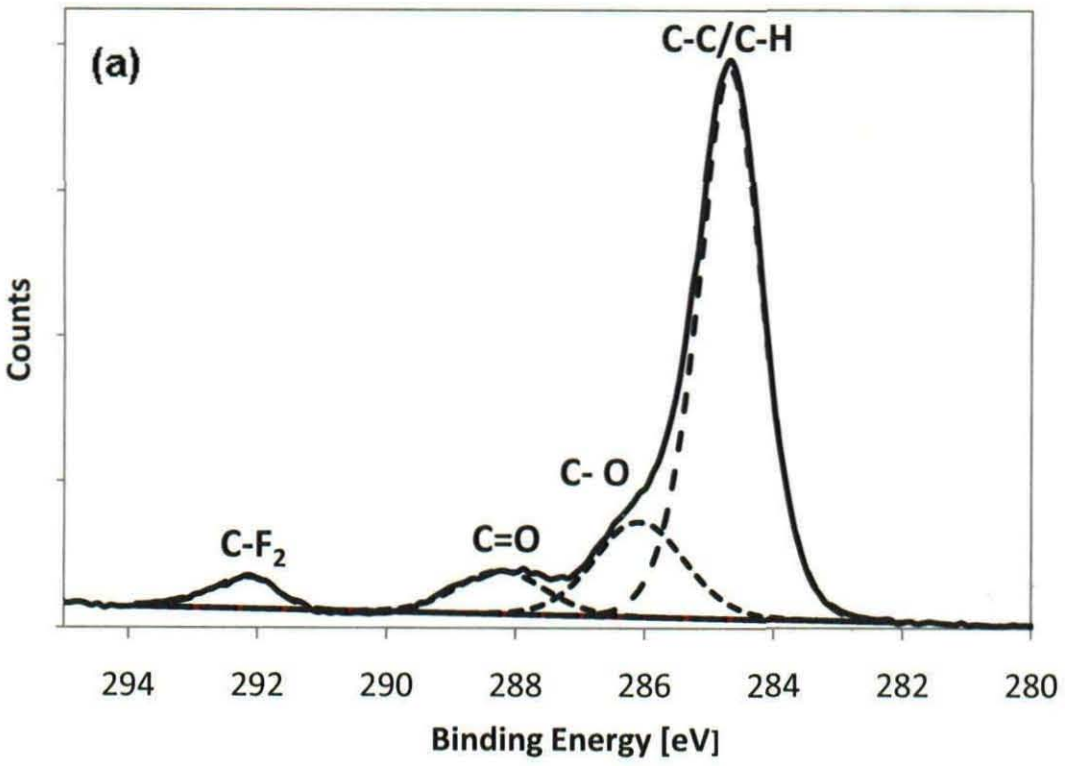
(a)
C-C/C-H
C- O
C=O
C-F2
Counts
294
292
290
288
286
284
282
280
Binding Energy [eV]

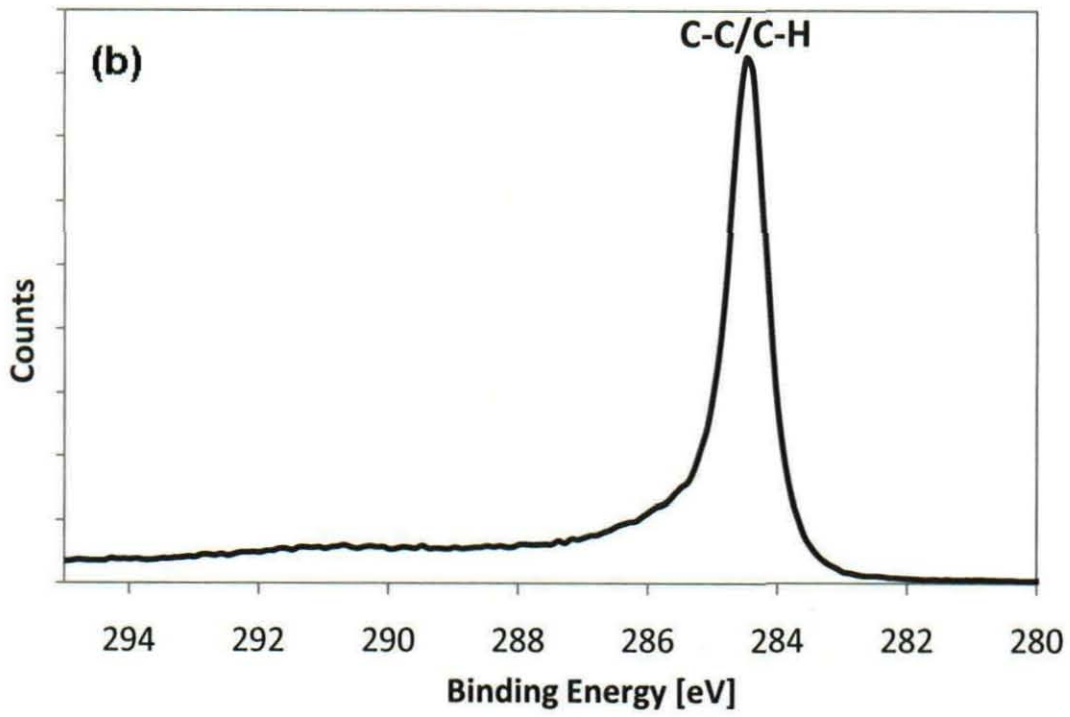
(b)
C-C/C-H
Counts
294
292
290
288
286
284
282
280
Binding Energy [eV]

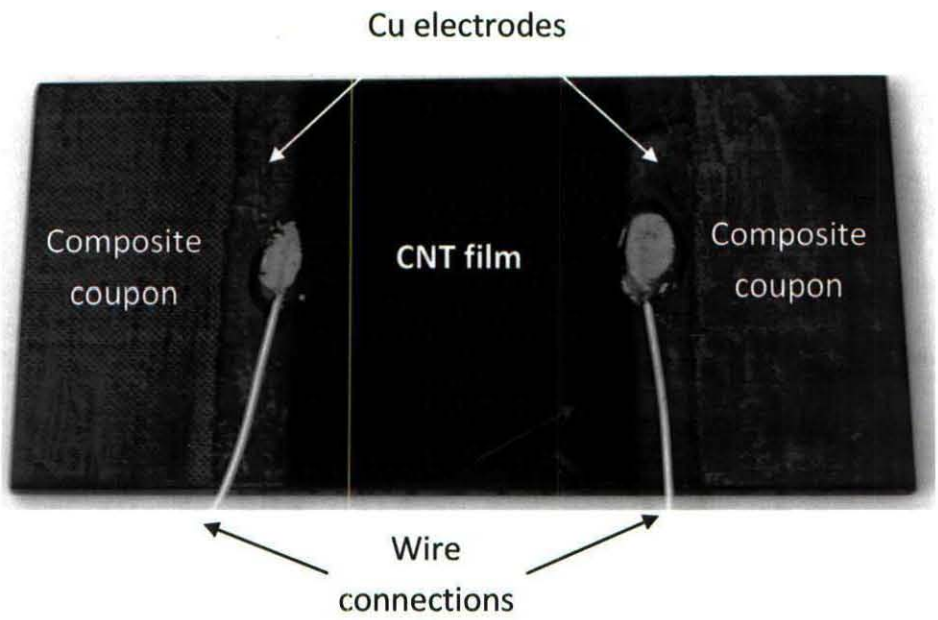
Cu electrodes
Composite coupon
CNT film
Composite coupon
Wire connections

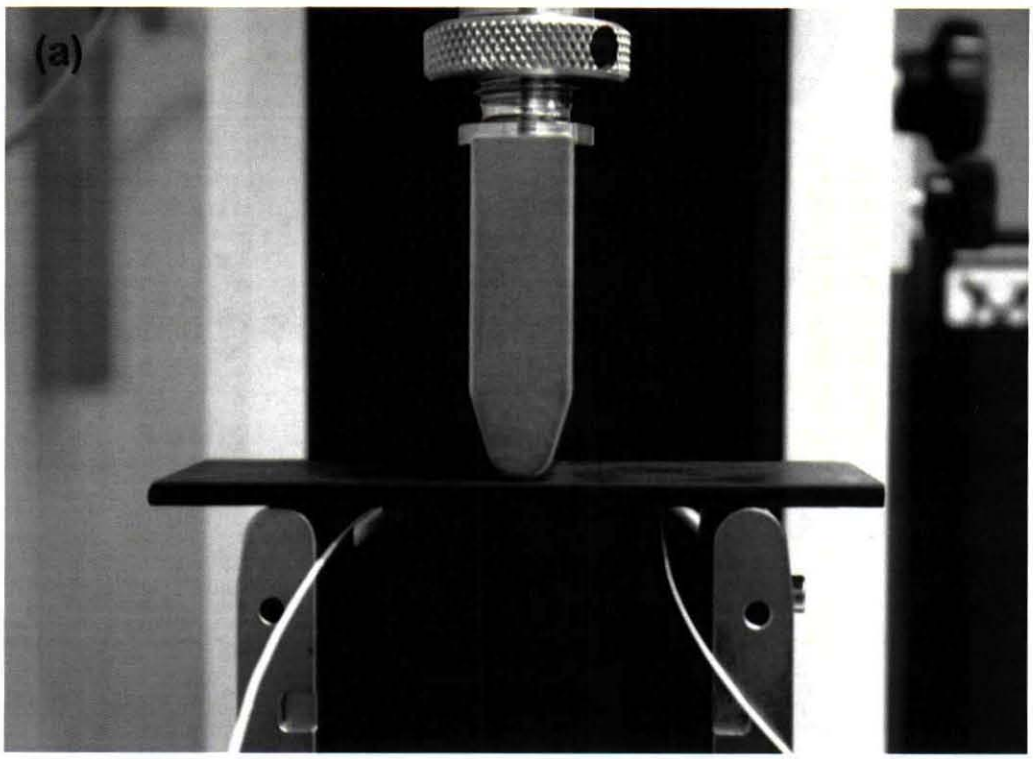
(a)

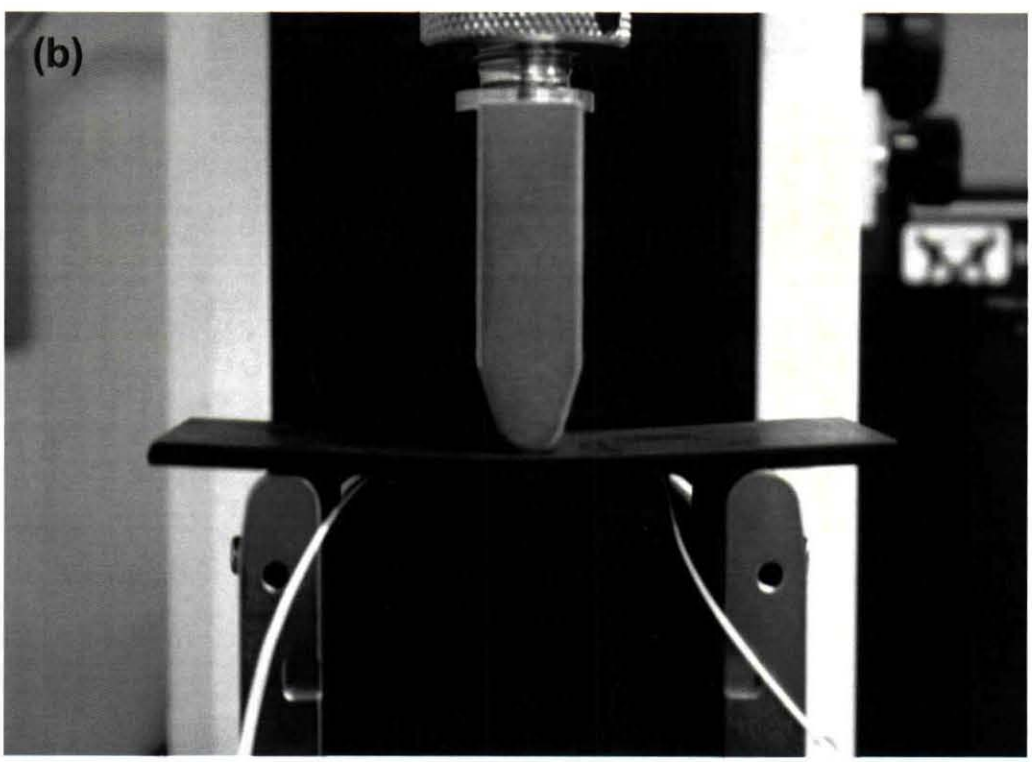
(b)

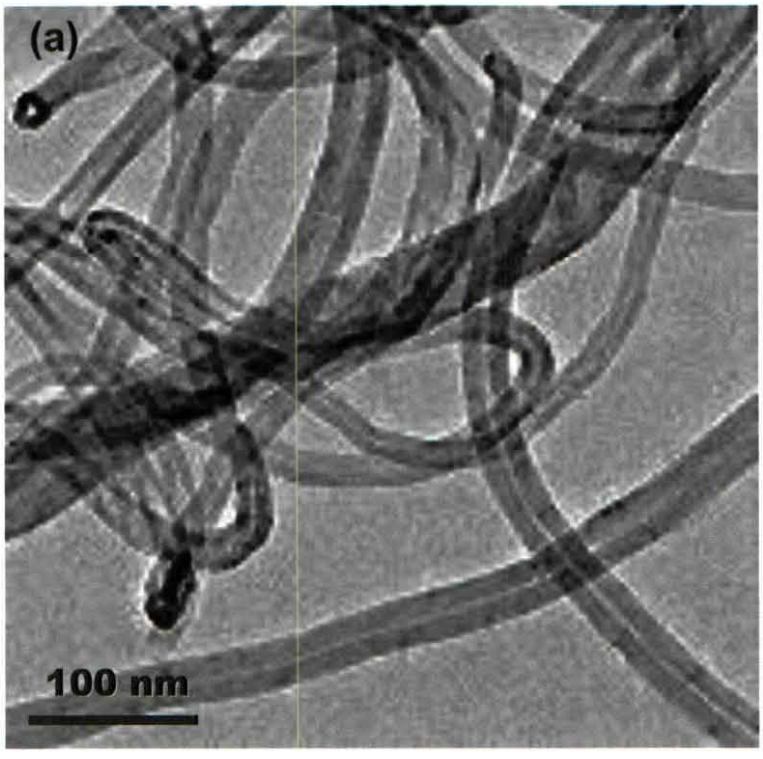
(a)
100 nm

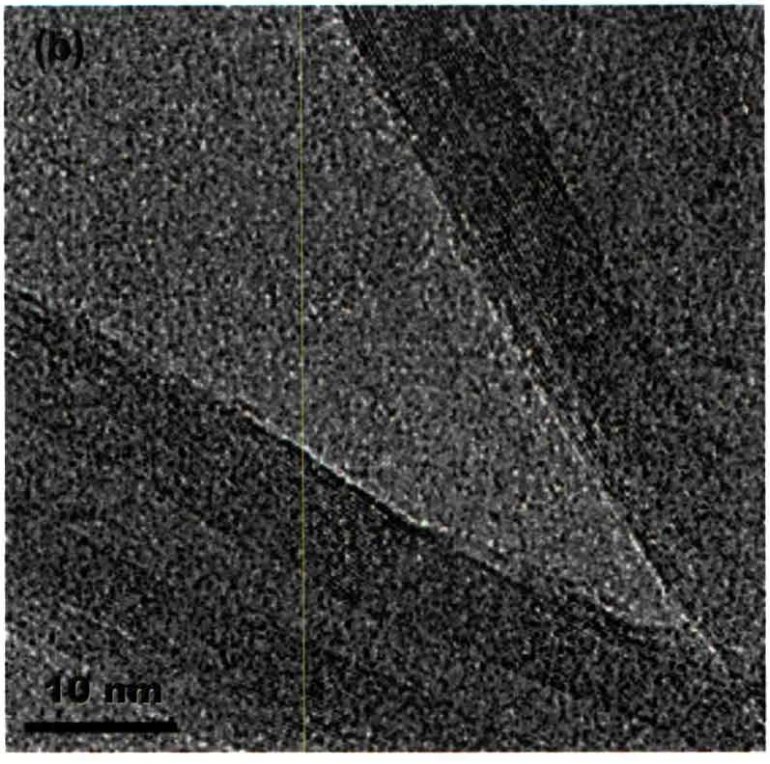
(b)
10 nm

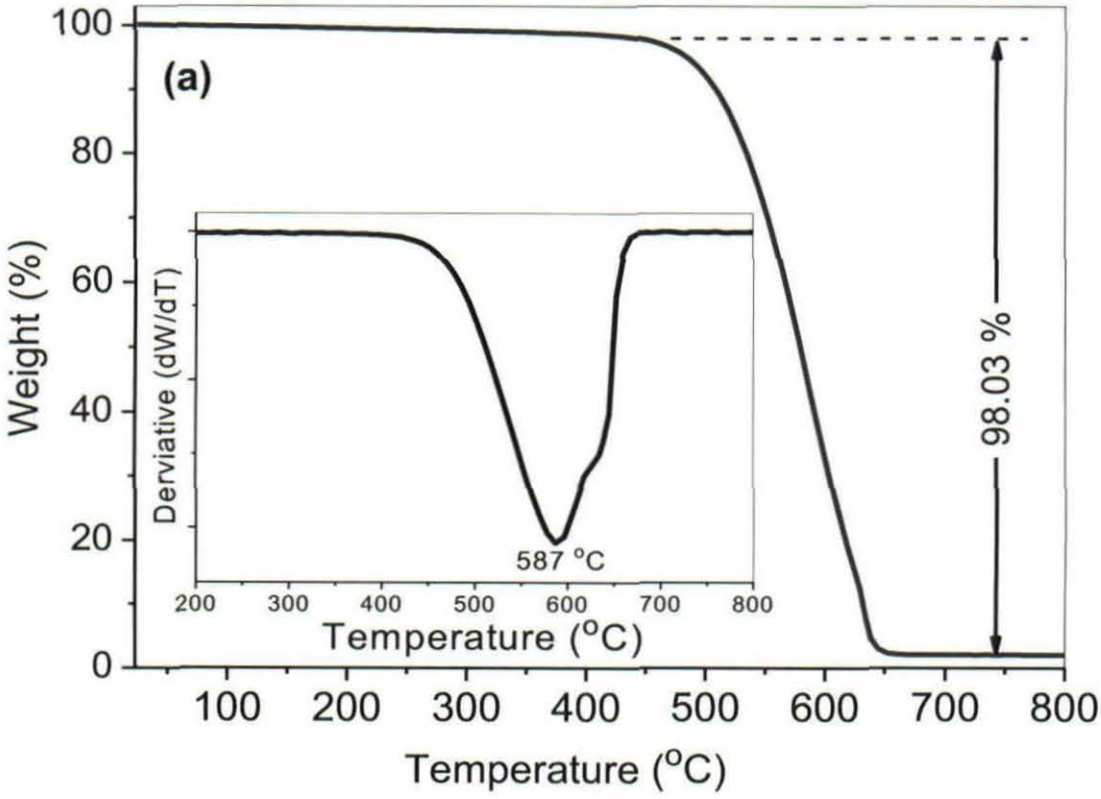
(a)
Weight (%)
Temperature (°C)
Derviative (dW/dT)
587 °C
98.03 %

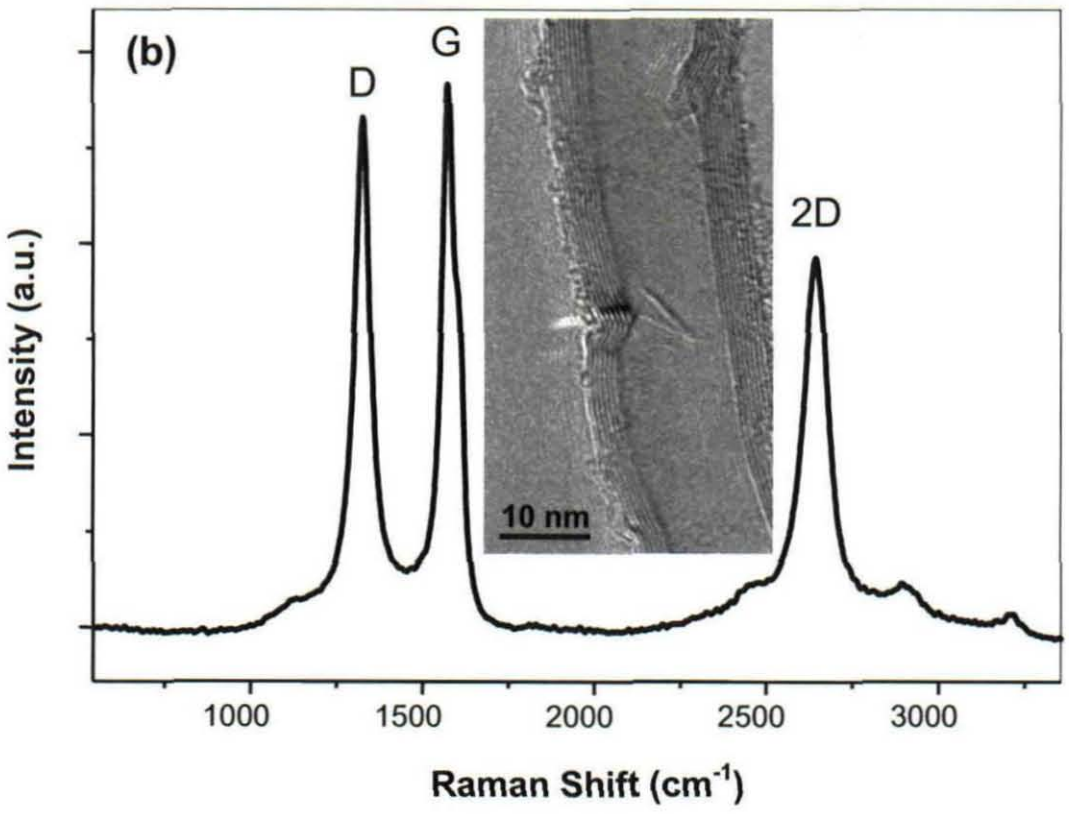
(b)
D
G
2D
10 nm
Intensity (a.u.)
Raman Shift (cm-1)

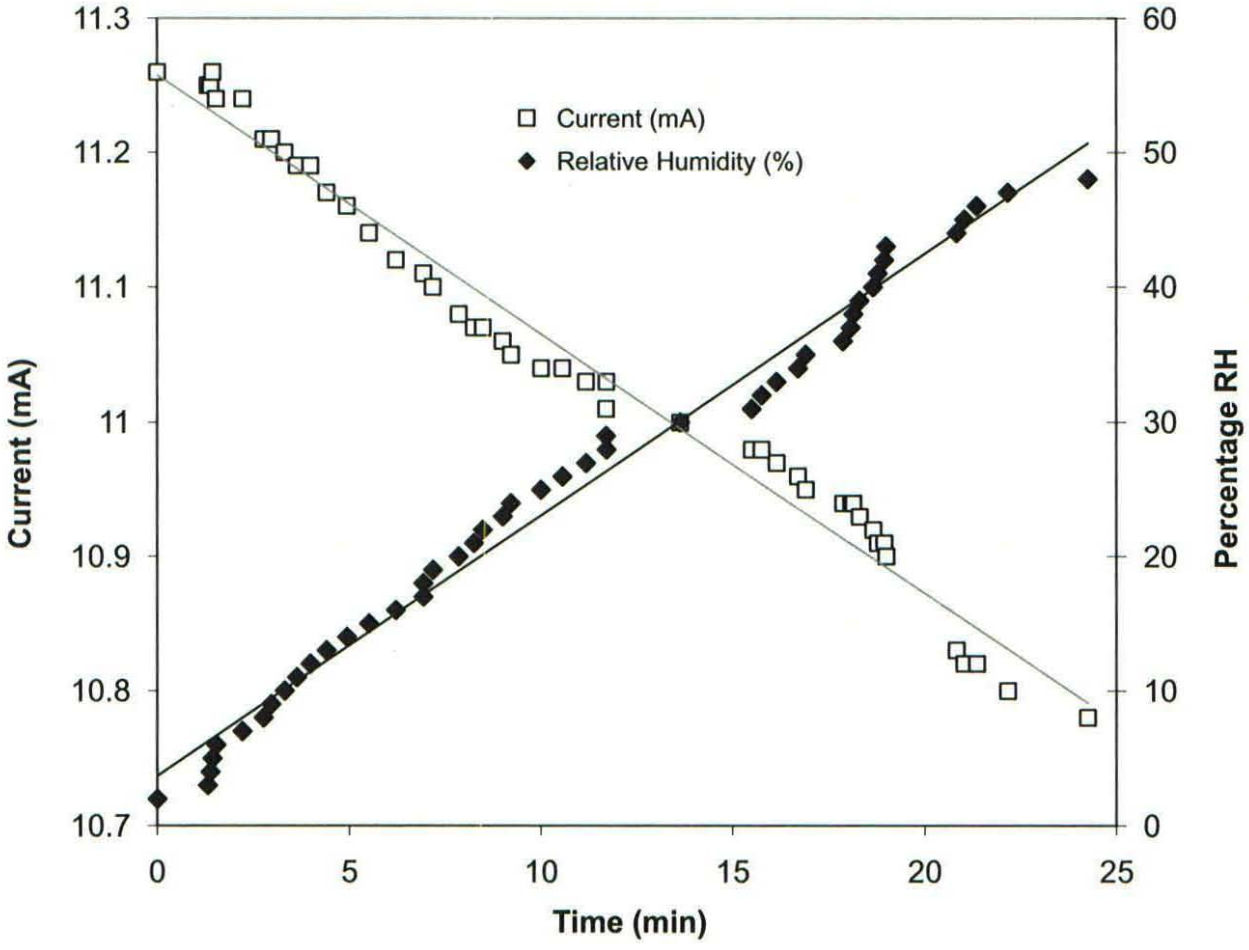
11.3
11.2
11.1
11
10.9
10.8
10.7
Current (mA)
60
50
40
30
20
10
0
Percentage RH
0
5
10
15
20
25
Time (min)
Current (mA)
Relative Humidity (%)

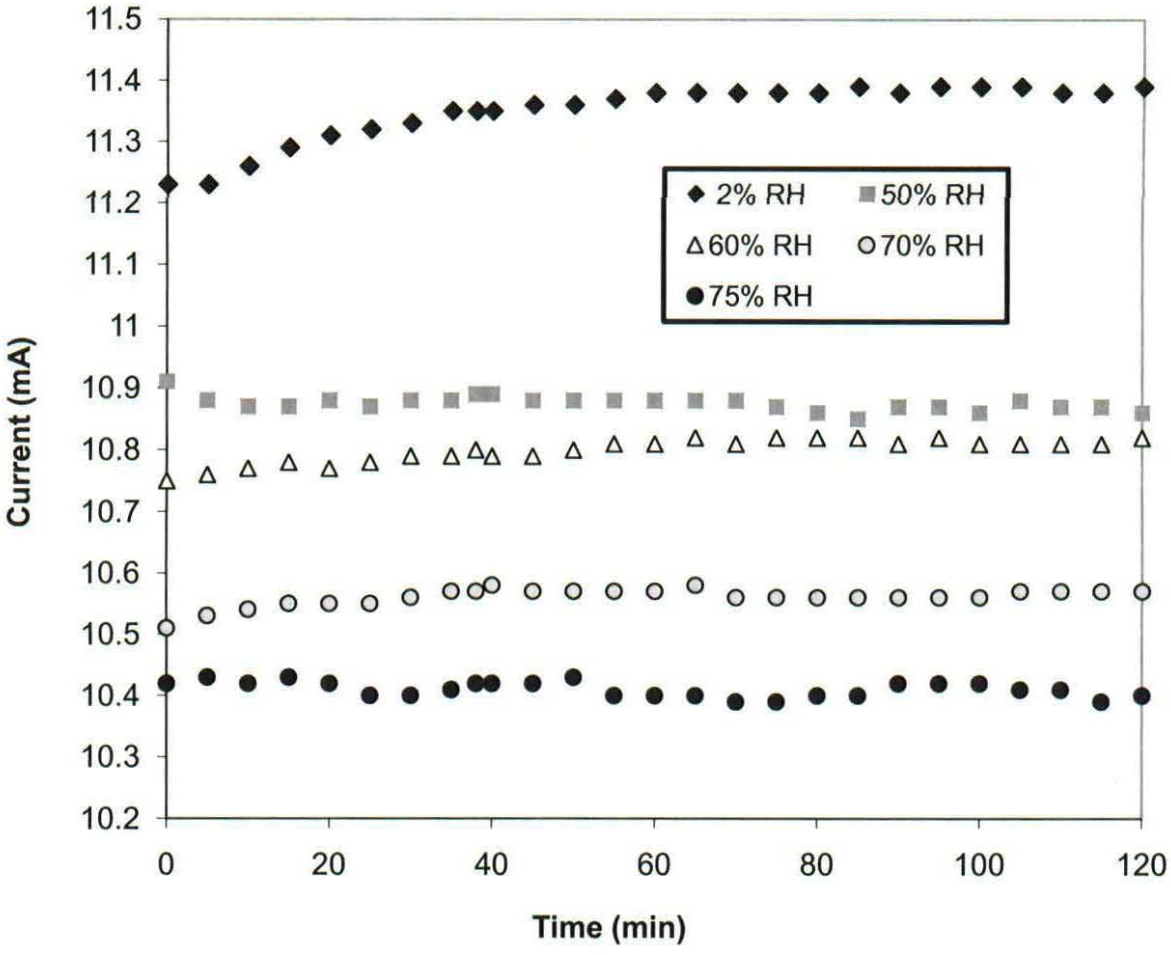
11.5
11.4
11.3
11.2
11.1
11
10.9
10.8
10.7
10.6
10.5
10.4
10.3
10.2
Current (mA)
0
20
40
60
80
100
120
Time (min)
2% RH
50% RH
60% RH
70% RH
75% RH

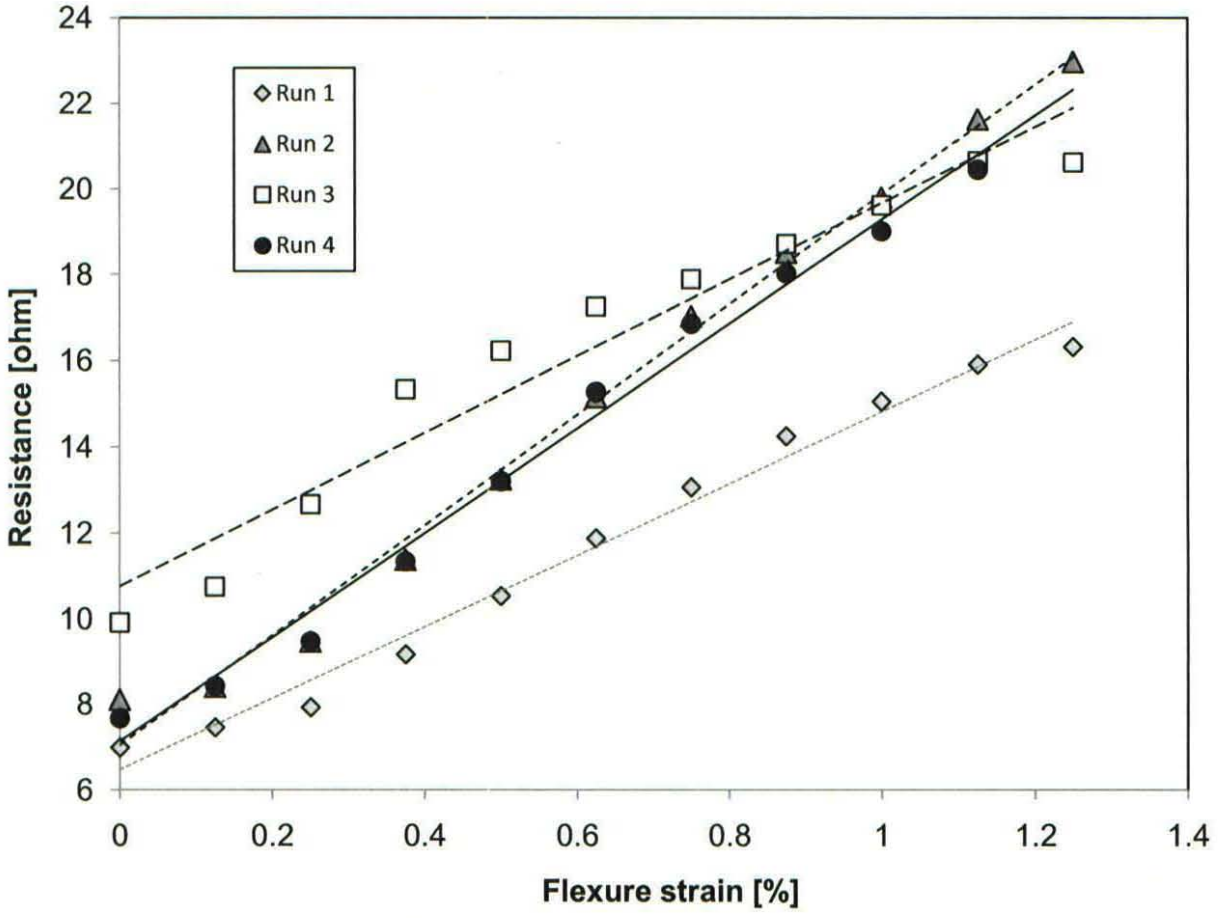
Run 1
Run 2
Run 3
Run 4
Resistance [ohm]
Flexure strain [%]
24
22
20
18
16
14
12
10
8
6
0
0.2
0.4
0.6
0.8
1
1.2
1.4

	Starting resistance [Ω]	Maximum resistance [Ω]	End resistance [Ω]
Run 1	6.99	16.32	7.04
Run 2	8.11	22.53	8.44
Run 3	9.91	20.94	7.92
Run 4	7.67	20.46	7.70

	C	O	F	N	Si	Zn	Na	S	Ca	Cl
Uncoated	65.9	19.0	7.7	2.3	1.6	1.3	0.95	0.54	0.49	0.23
Coated	96.2	3.8	-	-	-	-	-	-	-	-